Quasi-Direct Optical Transitions in Silicon Nanocrystals with Intensity Exceeding the Bulk

Benjamin G. Lee,[*,†] Jun-Wei Luo,[*,‡,§] Nathan R. Neale,[†] Matthew C. Beard,[†] Daniel Hiller,[∥] Margit Zacharias,[∥] Paul Stradins,[†] and Alex Zunger[⊥]

[†]National Renewable Energy Laboratory, Golden, Colorado 80401, United States

[‡]State Key Laboratory of Superlattices and Microstructures, Institute of Semiconductors, Chinese Academy of Sciences, Beijing 100083, China

[§]Synergetic Innovation Center of Quantum Information and Quantum Physics, University of Science and Technology of China, Hefei, Anhui 230026, China

[∥]Laboratory of Nanotechnology, IMTEK, Albert Ludwigs University, Freiburg 79110, Germany

[⊥]Renewable and Sustainable Energy Institute, University of Colorado, Boulder, Colorado 80309, United States

Supporting Information

Comparison of the measured absolute absorption cross section on a per Si atom basis of plasma-synthesized Si nanocrystals (NCs) with the absorption of bulk crystalline Si shows that while near the band edge the NC absorption is weaker than the bulk, yet above ∼2.2 eV the NC absorbs up to 5 times more than the bulk. Using atomistic screened pseudopotential calculations we show that this enhancement arises from interface-induced scattering that enhances the quasi-direct, zero-phonon transitions by mixing direct Γ-like wave function character into the indirect X-like conduction band states, as well as from space confinement that broadens the distribution of wave functions in k-space. The absorption enhancement factor increases exponentially with decreasing NC size and is correlated with the

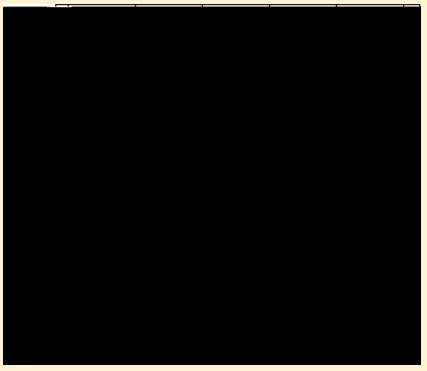

tum-forbidden to momentum allowed transitions as quasi-direct states, quantum confinement,[17] surface imperfections, and strain,[18] to name a few. We thus start by discussing the broader context of the underlying science that may lead to finite zero phonon transition intensity in NCs made of indirect gap solids.

As is well-known, each electronic state in translationally periodic crystalline solids can be classified by a single band $\{\phi_{n,}(\ ) = u_{n,}(\ )e^{i\cdot}\}$, belonging to a distinct wavevector $\boldsymbol{k}$ and band index n. Not surprisingly, the interband transitions between the valence and conduction bands are nonzero only if the wavevectors of the initial and final states are equal (momentum allowed direct transitions) in which case the intensity of the transition depends on the remaining factor, being the orbital character of the initial and final state with momentum (p) transition probability $P_{n_v n_c} = \langle u_{n_v \mathrm{k}}(\mathrm{r})|\hat{e}\cdot\mathrm{p}|u_{n_c \mathrm{k}}(\mathrm{r})\rangle$, reflecting the possibility of orbitally allowed vs orbitally forbidden transitions, associated with the point group selection rules. In contrast with such a relatively simple situation characterizing translationally periodic crystals, when translational periodicity is partially or fully removed, as is the case in nanostructures[19] or random bulk alloys,[20] then quantum mixing between the bulk Bloch states is allowed, and each nanostructure electronic state $\psi_{i,}(\ )$ is a superposition of the bulk Bloch functions of the underlying perfect crystals

$$\begin{aligned}\psi_{i\,\mathrm{K}}(\mathrm{r}) &= \frac{}{\sqrt{N}}\sum_{n}^{\infty}\sum_{\mathrm{k}}^{N_{\mathrm{k}}} c_{i\,n\,\mathrm{K}}(\mathrm{k})u_{n\,\mathrm{k}}(\mathrm{r})e^{i(\mathrm{k}+\mathrm{K})\cdot\mathrm{r}} \\ &= \frac{}{\sqrt{N}}\sum_{n}^{\infty}\sum_{\mathrm{k}}^{N_{\mathrm{k}}} c_{i\,n\,\mathrm{K}}(\mathrm{k})\phi_{n\,\mathrm{k}}(\mathrm{r})e^{i\mathrm{K}\cdot\mathrm{r}}\end{aligned} \tag{1}$$

belonging to a range of wavevectors and band indices n. Note that is a wavevector in the mini Brillouin zone of the superstructure, which is finite only for superstructures remaining partially translational periodic, such as 2D quantum wells and 1D nanowires, otherwise $\equiv 0$ and the symbol is then omitted—for example in 0D NCs. In this case the interband transition probability includes contributions from different wavevectors and different band components n of the underlying crystals:

$$\begin{aligned}\bar{P}_{v\,c} &= \langle\psi_{v\,\mathrm{K}_v}|\hat{e}\cdot\mathrm{p}|\psi_{c\,\mathrm{K}_c}\rangle \\ &= \frac{}{N}\sum_{n_v}^{\infty}\sum_{n_c}^{\infty}\sum_{\mathrm{k}_v}^{N_{\mathrm{k}}}\sum_{\mathrm{k}_c}^{N_{\mathrm{k}}} c^{*}_{v\,n_v\,\mathrm{K}_v}(\mathrm{k}_v)c_{c\,n_c\,\mathrm{K}_c}(\mathrm{k}_c) \\ &\quad \langle\phi_{n_v\,\mathrm{k}_v}|\hat{e}\cdot\mathrm{p}|\psi_{n_c\,\mathrm{k}_c}\rangle\delta_{\mathrm{K}_v\mathrm{K}_c} \\ &= \frac{}{N}\sum_{n_v}^{\infty}\sum_{n_c}^{\infty}\sum_{\mathrm{k}_v}^{N_{\mathrm{k}}}\sum_{\mathrm{k}_c}^{N_{\mathrm{k}}} c^{*}_{v\,n_v\,\mathrm{K}_v}(\mathrm{k}_v)c_{c\,n_c\,\mathrm{K}_c}(\mathrm{k}_c) \\ &\quad P_{n_v n_c}\delta_{\mathrm{k}_v\mathrm{k}_c}\delta_{\mathrm{K}_v\mathrm{K}_c}\end{aligned} \tag{2}$$

Here, $P_{n_v n_c} = \langle u_{n_v \mathrm{k}}(\mathrm{r})|\hat{e}\cdot\mathrm{p}|u_{n_c \mathrm{k}}(\mathrm{r})\rangle$ is the dipole matrix of bulk Si Bloch functions. It is well-established that the bulk Si crystal with its underlying tetrahedral point group symmetry has a momentum indirect bandgap transition (VBM at Γ-point and CBM at -point), which is forbidden because the one and only nonzero expansion coefficient of the VBM is at Γ-point but of the CBM is at -point. Together with the momentum conservation rule $\delta_{\mathrm{k}_v,\mathrm{k}_c}$, this leads to $\bar{P}_{v\,c} =$. To obtain finite transition intensity one could either focus on restoring momentum conservation by coupling the right phonon to break the condition of $\delta_{\mathrm{k}_v,\mathrm{k}_c}$ in eq 2 (a second order phonon assisted process which is generally weak and temperature-dependent[16]

measured.[2−10,12,13,23,26] However, a direct link was rarely established between these structural and chemical knobs and the degree of BFC created. Here we offer a simple computational tool that establishes such a link and in principle offers the design of effective BFC-inducing knobs.

Theoretical Methodology Used To Establish the Direct Transition. The idea is to compute in the first step rather precisely the electronic structure of the NC, treating it as a large molecule (rather than drawing its properties from a reference effective mass description). We do so by explicitly incorporating in the relevant Schrodinger equation

$$\left(-\frac{\hbar}{m}\nabla + V(\mathrm{r})\right)\psi_i(\mathrm{r}) = \epsilon_i\psi_i(\mathrm{r}) \tag{3}$$

with the crystal potential of the NC plus its matrix, both described as a superposition of atomic screened potentials υ_α of atom type α at each atomic site $R_{\alpha,n}$ within the lattice site n: $V(\ ) = \ _{\alpha,n}\upsilon_\alpha(\ -\ _{\alpha,n})$.[27] This superposition construct naturally includes (with atomic resolution) the positions of all atoms in the NC as well as the explicit surface ligands of interfaces. These define the various engineering knobs that may control the BFC, including volume quantum confinement, deviations from ideal T_d symmetry, surface, and interface effects, etc. This Schrodinger equation is solved numerically (in a plane wave basis set) providing the wave functions used in eq 2 to describe the interband transition intensity. In the second step, and for the purpose of analysis only, we expand the numerically precise NC wave functions by a set of Bloch states of underlying perfect Si crystal, as in eq 1. This gives us the spectral function telling if the specific engineering degrees of freedom used create sufficient Γ character to produce strong absorption. It is straightforward from eq 1 that if we sum over the bands n at a given first Brillouin zone wavevector , we obtain the "majority representation" decomposition of the QD state i as[20]

$$p_i(\mathrm{k}) = \sum_n |\langle\psi_i(\mathrm{r})|u_{n\,\mathrm{k}}e^{i\mathrm{k}\cdot\mathrm{r}}\rangle| \tag{4}$$

This quantity describes the amplitude of the bulk Bloch functions at any wavevector as it mixes into the quantum state (VBM, CBM, etc.) i and will be shown below in Figure 4. It thus supplies a direct link between structural or chemical engineering knobs (specified in the NC potential $V(\ )$) and the ensuing state mixing accomplished. An auxiliary quantity useful for analysis is the weight functions ω_i^Γ, ω_i^X, and ω_i^L, which are defined by summing $p_i(\ )$ over the k points contained in a spherical region around Γ

$$E = \frac{\varepsilon}{\varepsilon + \varepsilon} E \tag{8}$$

Thus, the absorption of the sphere is also reduced:

$$= -\langle D \cdot \frac{E}{t} \rangle \sim \frac{n}{n} \left(\frac{\varepsilon}{\varepsilon + \varepsilon} \right) \tag{9}$$

Note that the derived absorption is proportional to the volume of the nanoparticle; thus when normalized to a per Si atom basis, the same correction factor applies for all particle radii.

Moreover, the per Si atom normalization is more accurate than normalizing to average NC size, since there is variability in the NC diameter within each sample, in addition to the inherent uncertainty in the size determination. The per Si atom normalized optical absorption of NCs compared with (local bulk field factor corrected) bulk c-Si is shown in Figure 3.

We find two

Significantly, even for larger NCs (e.g., 4 nm size) we see appreciable Γ-component in the conduction band states. Specifically, the presence of Γ-component exists in numerous states below 3.4 eV (Γ−Γ transition in bulk Si). Thus, there is increased likelihood of quasi-direct optical transitions. This quasi-direct character can be seen in the calculated zero-phonon optical absorption (Figure 5b) of 3 and 4 nm diameter NCs; this calculation excludes all phonon-assisted processes, showing only quasi-direct transitions. It is clear from these calculations that zero-phonon transitions are allowed at much lower energies for quantum-confined NCs than in bulk Si.

The momentum conservation law of optical transition, which forces the band gap transition of bulk Si to be strictly forbidden, is partially relaxed in Si NCs leading to the enhancement of optical transition in Si NCs. This relaxation was attributed earlier to the Heisenberg uncertainty principle $r \cdot k > 1/2$, where r is the NC radius and k is the wavevector of QD electrons or holes.[37] This is a result of space reduction in a NC leading to a spread in momentum, a spread that induces the possibility of the overlap of electron and hole wave function in k-space and thus allows the optical transitions (eq 2). This mechanism alone would predict that the k-space wave function of the CBM (VBM) in Si NCs should be mostly centered at the -point (Γ-point) and exponentially decay away from there. The extent of the spread is inversely proportional to the NC size. Along with the k-space spread of wave functions, the space confinement also increases the energy of quantized states as the NC size is reduced (to the power of 1−2).[25] Thus, the quantum confinement should result in a power law scale of light emission and confinement energy on NC size. These features of space quantum confinement effects are in excellent agreement with that of our atomistic pseudopotential calculated results for Si NCs, as shown in Figure 5a and b.

This agreement demonstrates that the space confinement dominates the relaxation of momentum conservation for Si NCs. However, the space confinement effect is not the only cause of the spread of the wave function. We propose a mechanism, where the spread of electron and hole wave functions arises from scattering at the interface causing Γ−X intervalley coupling, giving an admixture of Γ-character to X-valley dominated conduction band states, and enabling an increase in quasi-direct transitions. This line of reasoning is bolstered by the results of our recent work[1] to reveal specific Si/Ge superlattices (e.g., α-sequence $SiGe_2Si_2Ge_2SiGe_{12}$ super-

conduction band states of the NC core have a mix of X- and Γ-character. This appreciable Γ-component permits zero-phonon, quasi-direct optical transitions in the Si NCs, at energies between the quantum-confined band gap in NCs and the bulk c-Si direct band gap at 3.4 eV. This helps explain the experimentally observed enhanced absorption between ∼2.2 and 3.4 eV for quantum-confined Si NC samples.

■ ASSOCIATED CONTENT

Supporting Information

The Supporting Information is available free of charge on the ACS Publications website at DOI: 10.1021/acs.nanolett.5b04256.

Details of synthesis/preparation and measurements of Si nanocrystal samples, including both plasma-synthesized Si NCs and Si NCs in oxide matrix (PDF)

■ AUTHOR INFORMATION

Corresponding Authors

*E-mail: benjamin.lee@nrel.gov.
*E-mail: jwluo@semi.ac.cn.

Author Contributions

Both corresponding authors contributed equally to the paper.

Notes

The authors declare no competing financial interest.

■ ACKNOWLEDGMENTS

We thank H.M. Branz (NREL) for discussions and I. Anderson for initial sample fabrication. B.G.L. and P.S. acknowledge support by the US Department of Energy Solar Energy Technology Program under Contract No. DE-AC36-99GO10337. J.W.L. was supported by the National Young 1000 Talents Plan and the National Science Foundation of China (NSFC grant #61474116). N.R.N. and M.C.B. were funded by the Solar Photochemistry Program of the Division of Chemical Sciences, Geosciences, and Biosciences, Office of Basic Energy Sciences, of the U.S. Department of Energy under Contract No. DE-AC36-08-GO28308. Work of A.Z. was supported by Department of Energy, Office of Science, Basic Energy Science, MSE division under grant DE-FG02-13ER46959 to CU Boulder. D.H. and M.Z. acknowledge financial support by DFG (HI 1779/3-1).

■ REFERENCES

(1) d'Avezac, M.; Luo, J.-W.; Chanier, T.; Zunger, A. Phys. Rev. Lett. **0** , 108 (2), 027401.
(2) Furukawa, S.; Miyasato, T. Phys. Rev. B: Condens. Matter Mater. Phys. , 38 (8), 5726.
(3) Canham, L. T. Appl. Phys. Lett. **0**, 57 (10), 1046−1048.
(4) Lehmann, V.; Gosele, U. Appl. Phys. Lett. , 58 (8), 856−858.
(5) Baehr-Jones, T.; Pinguet, T.; Guo-Qiang, P. L.; Danziger, S.; Prather, D.; Hochberg, M. Nat. Photonics **0** , 6 (4), 206−208.
(6) Iyer, S. S.; Xie, Y.-H. Science , 260 (5104), 40−46.
(7) Asghari, M.; Krishnamoorthy, A. V. Nat. Photonics **0** , 5 (5), 268−270.
(8) Ng, W. L.; Lourenco, M. A.; Gwilliam, R. M.; Ledain, S.; Shao, G.; Homewood, K. P. Nature **00** , 410 (6825), 192−194.
(9) Green, M. A.; Zhao, J.; Wang, A.; Reece, P. J.; Gal, M. Nature **00** , 412 (6849), 805−808.
(10) Hirschman, K. D.; Tsybeskov, L.; Duttagupta, S. P.; Fauchet, P. Nature , 384 (6607), 338−341.
(11) Meier, C.; Gondorf, A.; Luttjohann, S.; Lorke, A.; Wiggers, H. J. Appl. Phys. **00** , 101 (10), 103112.
(12) Holmes, J. D.; Ziegler, K. J.; Doty, R. C.; Pell, L. E.; Johnston, K. P.; Korgel, B. A. J. Am. Chem. Soc. **00** , 123 (16), 3743−3748.
(13) Gresback, R.; Murakami, Y.; Ding, Y.; Yamada, R.; Okazaki, K.; Nozaki, T. Langmuir **0** , 29 (6), 1802−1807.
(14) Mustafeez, W.; Majumdar, A.; Vuckovic, J.; Salleo, A. J. Appl. Phys. **0** , 115 (10), 103515.
(15) Kovalev, D.; Diener, J.; Heckler, H.; Polisski, G.; Kunzner, N.; Koch, F. Phys. Rev. B: Condens. Matter Mater. Phys. **000**, 61 (7), 4485−4487.
(16) Hybertsen, M. S. Phys. Rev. Lett. , 72 (10), 1514.
(17) Delley, B.; Steigmeier, E. F. Phys. Rev. B: Condens. Matter Mater. Phys. , 47 (3), 1397−1400.
(18) Lee, B. G.; Hiller, D.; Luo, J.-W.; Semonin, O. E.; Beard, M. C.; Zacharias, M.; Stradins, P. Adv. Funct. Mater. **0** , 22